Journal of Anatomy

J. Anat. (2018) **233**, pp86–97 doi: 10.1111/joa.12817

Nerves and blood vessels in degenerated intervertebral discs are confined to physically disrupted tissue

Polly Lama,[1] Christine L. Le Maitre,[2] Ian J. Harding,[3] Patricia Dolan[4] and Michael A. Adams[4]

[1]*Department of Orthopaedic Surgery, McGill University, Montreal, QC, Canada*
[2]*Biomolecular Sciences Research Centre, Sheffield Hallam University, Sheffield, UK*
[3]*Southmead Hospital, Bristol, UK*
[4]*Centre for Applied Anatomy, University of Bristol, Bristol, UK*

Abstract

Nerves and blood vessels are found in the peripheral annulus and endplates of healthy adult intervertebral discs. Degenerative changes can allow these vessels to grow inwards and become associated with discogenic pain, but it is not yet clear how far, and why, they grow in. Previously we have shown that physical disruption of the disc matrix, which is a defining feature of disc degeneration, creates free surfaces which lose proteoglycans and water, and so become physically and chemically conducive to cell migration. We now hypothesise that blood vessels and nerves in degenerated discs are confined to such disrupted tissue. Whole lumbar discs were obtained from 40 patients (aged 37–75 years) undergoing surgery for disc herniation, disc degeneration with spondylolisthesis or adolescent scoliosis ('non-degenerated' controls). Thin (5-μm) sections were stained with H&E and toluidine blue for semi-quantitative assessment of blood vessels, fissures and proteoglycan loss. Ten thick (30-μm) frozen sections from each disc were immunostained for CD31 (an endothelial cell marker), PGP 9.5 and Substance P (general and nociceptive nerve markers, respectively) and examined by confocal microscopy. Volocity image analysis software was used to calculate the cross-sectional area of each labelled structure, and its distance from the nearest free surface (disc periphery or internal fissure). Results showed that nerves and blood vessels were confined to proteoglycan-depleted regions of disrupted annulus. The maximum distance of any blood vessel or nerve from the nearest free surface was 888 and 247 μm, respectively. Blood vessels were greater in number, grew deeper, and occupied more area than nerves. The density of labelled blood vessels and nerves increased significantly with Pfirrmann grade of disc degeneration and with local proteoglycan loss. Analysing multiple thick sections with fluorescent markers on a confocal microscope allows reliable detection of thin filamentous structures, even within a dense matrix. We conclude that, in degenerated and herniated discs, blood vessels and nerves are confined to proteoglycan-depleted regions of disrupted tissue, especially within annulus fissures.

Key words: blood vessels; degeneration; free surfaces; ingrowth; intervertebral discs; nerves.

Introduction

The risk of severe and chronic back pain increases with increasing lumbar disc degeneration (Cheung et al. 2009). However, many 'degenerative' changes seen on magnetic resonance imaging (MRI), such as proteoglycan and water loss, or minor disc bulging, have little relationship to pain (Boden et al. 1990; Boos et al. 1995) and are best understood as the more or less inevitable consequences of disc ageing (Boos et al. 2002; Vo et al. 2016). In contrast, the risk of back pain is substantially increased by specific structural changes in the annulus and endplate, such as radial fissures in the annulus (Videman & Nurminen, 2004), major disc herniations (Boos et al. 1995), endplate defects (Wang et al. 2012) and their associated Modic changes (Maatta et al. 2016), and disc narrowing (de Schepper et al. 2010).

Underlying mechanisms in discogenic pain are not clear but probably involve the ingrowth of blood vessels and nerves (Aoki et al. 2004), which normally are confined to the disc periphery (Ashton et al. 1994a; Coppes et al. 1997; Freemont et al. 1997; Peng et al. 2005). Fine nerves in the peripheral posterior and posterolateral annulus arise from the mixed sinuvertebral nerve and are believed to be capable of nociception (Bogduk et al. 1981). Some of them associate with blood vessels within granulation tissue

Correspondence
Polly Lama, Department of Orthopaedic Surgery Research, McGill University, 1650 Cedar Avenue, Montreal, QC, Canada H3G 1A4.
T: +1-514-756-6069; E: polly.lama@mail.mcgill.ca

Accepted for publication *2 April 2018*
Article published online *30 April 2018*

(Ashton et al. 1994a), and are probably capable of mechanoreception and nociception (Roberts et al. 1995; Aoki et al. 2004). Nerve ingrowth may be stimulated and guided by growth factors such as NGF which are secreted by blood vessels and disc cells (Freemont et al. 2002; Purmessur et al. 2008; Tolofari et al. 2010). However, the ingrowth of blood vessels is more problematic because they are effectively hollow tubes that would be collapsed by the high fluid pressures found inside the nucleus and middle annulus of adult human discs (Adams et al. 1996b).

In previous work we showed that annulus fissures are physically and chemically conducive to blood vessel ingrowth because they represent a micro-environment of low physical pressure (Stefanakis et al. 2012). Furthermore, the walls of annulus fissures are effectively 'free surfaces' which enable focal swelling and proteoglycan loss (Stefanakis et al. 2012), leaving collagen-rich surfaces that facilitate cell migration. Certainly, high proteoglycan concentrations inhibit growth of blood vessels and nerves *in vitro* (Johnson et al. 2002, 2005; Purmessur et al. 2015). As a result of these physical and chemical influences, blood vessels are generally excluded from the nucleus and inner annulus regions of human discs, even when they are degenerated (Nerlich et al. 2007), although they can grow into focal defects (Peng et al. 2005; Nerlich et al. 2007). Animal 'injury' models of disc degeneration also report nerves growing into annulus defects (Xin et al. 2017), and sensory innervation increases in disrupted human endplates (Fields et al. 2014).

In summary, we know already that nerves and blood vessels can grow into physically disrupted disc tissue with a low proteoglycan content. We now hypothesise that *all* ingrowth occurs in such tissue, and nowhere else. If this hypothesis is supported, it will help clinicians to locate nerves within painful intervertebral discs, and to relieve discogenic pain.

To ensure clinical relevance, we studied surgically removed tissues from patients believed to have discogenic pain. To maximise our ability to detect fine nerves within a dense and extensive matrix, we examined multiple thick sections using confocal microscopy and immunofluorescence. Specific objectives were to: (1) characterise the spatial distribution of blood vessels using general histological stains applied to 5-μm-thin sections; (2) quantify blood vessels and nerves in 30-μm-thick frozen sections, using confocal microscopy and immunofluorescence; (3) determine whether the density of blood vessels and nerves depends on focal proteoglycan loss and the presence of free surfaces within disrupted tissue; and (4) correlate our findings with MRI-graded disc degeneration.

Materials and methods

Specimen collection

Following NRES (UK) ethical approval, posterolateral disc specimens were removed at surgery from 40 patients with one of the following diagnoses: herniated disc with sciatica (HD/S, $n = 10$); herniated disc without sciatica (HD/NS, $n = 11$); degenerated disc with spondylolisthesis (D&S, $n = 11$); and adolescent scoliosis (SD, $n = 8$). The last group were considered 'controls' with minimal degeneration. HD samples were primarily displaced nucleus plus annulus tissues, sometimes incorporating some cartilage endplate also, as described previously (Lama et al. 2013). D&S patients were undergoing surgery primarily for back pain, although in most cases, no exact pain source had been identified. Specimens were collected within 20 min of surgery and placed on dry ice. Subsequent defrosting allowed small adjacent blocks of tissue to be prepared and alternately allocated to fixation in formalin (for histology) or acetone (for immunofluorescence). Patients' MRI scans were obtained so that disc degeneration could be scored on a scale of 1–6 (Pfirrmann et al. 2001). Specimen details are summarised in Table 1.

Histology

Tissue blocks were fixed in 10% neutral buffered formalin and embedded in O.C.T. (optimal cutting tissue medium). Thin (5-μm) sections were cut at a high angle to the annulus lamellae (i.e. in the approximate sagittal and axial planes). They were then treated with Ehrlich's Haematoxylin & Eosin (H&E) stain for assessing cell types, and structures such as matrix fissures and blood vessels. Toluidine blue stain was used to derive a semi-quantitative measure of glycosaminoglycans (GAG) loss GAGs are the active, water-attracting components of proteoglycan molecules. Three fields of view were selected from each tissue type (see below). All stained sections were observed under a Leica light microscope with 20× and 40× objectives, and graded for histological degenerative scores based on a modified Boos scale (Boos et al. 2002) as described in Table 2.

Tissue characterisation

As described previously (Lama et al. 2013) three tissue types were distinguished histologically: nucleus pulposus (NP), inner annulus fibrosus (IAF) and outer annulus fibrosus (OAF). OAF tissue (Fig. 1) comprised highly organised type I collagen fibres with elongated fibroblast-like cells running parallel to the annulus lamellae. These collagen fibres are birefringent when viewed under polarised light and have high affinity for eosin stain. IAF tissue (Fig. 2) comprised wider and less organised annulus lamellae with numerous clusters of rounded cells, and with diminished birefringence and eosin staining. NP tissue (Fig. 3) had an amorphous collagen-poor but GAG-rich matrix, did not exhibit birefringence, and showed rounded chondrocyte-like cells in clusters or pairs (Freemont et al. 1997; Bruehlmann et al. 2002).

Immunofluorescence staining

Tissue blocks were fixed in acetone, cooled at −20 °C for 10 min, and thick (30-μm) sections were obtained using a cryostat. Sections were rinsed in phosphate-buffered saline (PBS) and treated with 20% donkey serum (Invitrogen, UK) in PBS for 60 min at 4 °C. Sections were washed in three changes of PBS and treated with mouse monoclonal primary antibodies at 1 : 25 dilutions in PBS for PGP 9.5 (general cytoplasmic neuronal marker, ABD Sorotec, UK), 1 : 20 dilution for CD 31 (endothelial cell marker; Dako, UK) and 1 : 500 dilutions for Substance P (nociceptive neuropeptides marker; Abcam, UK). We have shown previously that these antibodies are effective in labelling nerves and blood vessels in human

Table 1 Details of the disc specimens from four patient groups.

	Herniated discs – with sciatica (HD/S)	Herniated discs – no sciatica (HD/NS)	Degenerated and spondylolisthesis discs (D&S)	Adolescent scoliosis discs (SD)
n	10	11	11	8
Mean age (years)	51 (range 37–68)	53 (range 35–74)	53 (range 39–72)	15 (range 14–15)
Spinal level (*n*)	L2-3 (1), L3-4 (1), L4-5 (4), L5-S1 (4)	L3-4 (1), L4-5 (2), L5-S1 (8)	L2-3 (1), L3-4 (1), L4-5 (5), L5-S1 (4)	T12-L1 (1), L1-2 (2), L2-3 (2), L3-4 (2), L4-5 (1)
Gender (*n*)	M (2), F (8)	M (6), F (5)	M (5), F (6)	F (8)
Pfirrmann grade	3.5 (range 3–5)	3.4 (range 2–4)	3.0 (range 2–4)	1
Pain (months)	20 (range 2–60)	8 (range 3–18)	18 (range 4–60)	No pain

Table 2 Variables for histological assessment of discs, based on a modified Boos scale (Boos et al. 2002).

Histological variable	Grades
Neovascularity/blood vessels Newly formed blood vessels with reparative alterations	0 = absent 1 = rarely present 2 = present in intermediate amounts 3 = abundant
Tears/fissures Splitting of collagen fibre bundles in the annulus fibrosus and nucleus regions creating a gap or break within the tissue	0 = absent 1 = rarely present 2 = present in intermediate amounts 3 = abundant
GAG depletion Areas with loss of toluidine blue staining for GAG	0 = absent 1 = rarely present 2 = present in intermediate amounts 3 = abundant
Inflammatory cells Immunocytes with small irregular nuclei, often in swarms along the edges of/surfaces of disc tissue	0 = absent 1 = rarely present 2 = present in intermediate amounts 3 = abundant

intervertebral discs (Lama et al. 2013). Secondary donkey anti-mouse antibody was conjugated with Alexa-Fluorophore® (Invitrogen) and used at 1 : 200 dilutions in PBS. To quench autofluorescence, sections were immersed in 0.1% Sudan black B for 5 min (Baschong et al. 2001). Sections were then washed in PBS, counterstained and mounted with 4′,6-diamidino-2-phenylindole (DAPI; Vector Laboratories, UK). The excitation/emission spectrum for the secondary antibody was at 550/607 nm. For DAPI-stained nuclei, excitation was at 405 nm and emission at 488 nm. Primary antibodies were omitted during the incubation stage in the case of negative controls.

Ten 30-μm-thick sections were examined from each disc specimen. Depending on the section, three fields of view were taken each of NP, IAF and OAF tissue regions per section. Immunoreactive nerves and blood vessels were observed primarily with 20× magnification, but for good quality images 40× objective magnification was also used. Digital images were obtained using a Leica DMIRBE argon laser confocal scanning inverted microscope. All sections were sequentially scanned to prevent crosstalk between different fluorophores. To prevent photobleaching, a 4-line average was used for each image. Line average scans were useful in improving signal-to-noise ratio.

Quantification of blood vessels and nerves

The confocal microscope was used to identify all free surfaces, including the disc periphery and those within matrix fissures. Then, the shortest distance was measured (in μm) between each distinct (fragment of) blood vessel or nerve to the nearest free surface, using the 'line tool' of VOLOCITY 3-D image analysis software (Perkin Elmer). For blood vessels, a freehand region of interest (ROI) tool was used to outline each distinct fragment so that the software could calculate its cross-sectional area in μm^2. Each (fragment of) blood vessel or nerve identified by the software was uniquely colour-coded and numbered so that it would not be re-counted. For each tissue type and each patient group, mean values were calculated together with the standard deviation (SD) and the range. Separate data were obtained for immunoreactivity to PGP 9.5, Substance P and CD-31.

Statistical analysis

Ordinal data (grades) were averaged across multiple sections to obtain numerical data. This was acceptably normal, so one-way ANOVA was used to compare mean values of histological, immunohistochemical and radiological grades between (1) the three tissues of interest (NP, IAF and OAF) and (2) the four patient groups. Two-way ANOVA was used to examine interactions between tissue types and patient groups. Associations between histological variables were analysed using Spearman rank correlation. All statistical tests were executed using SPSS software version 18. $P < 0.05$ implied statistical significance.

Results

Histological differences between discs from four patient groups

Discs from adolescent scoliosis patients appeared normal (Figs 1A, 2A and 3A), whereas herniated and degenerated discs had highly disorganized collagen lamellae in the OAF (Fig. 1B). Disrupted areas were frequently infiltrated by

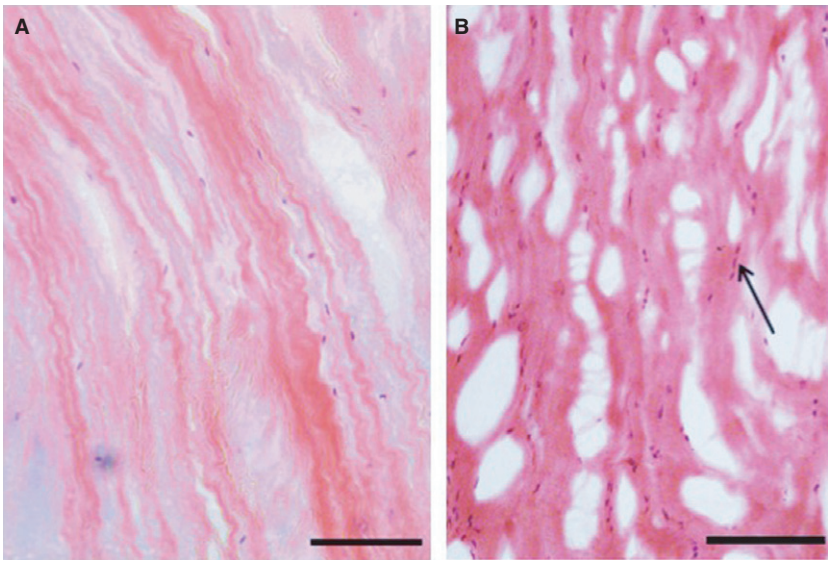

Fig. 1 Outer annulus fibrosus (OAF) tissue stained with H&E. (A) Non-degenerated scoliotic disc. Scale bar: 200 μm. (B) Degenerated spondylolisthesis disc. Scale bar: 100 μm. Note the elongated fibroblast-like cells (arrows) aligned with the crimped collagen fibres, and the numerous microscopic tears and splits in (B).

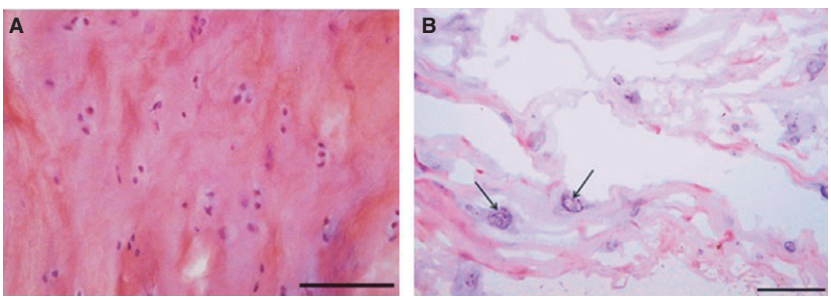

Fig. 2 Inner annulus fibrosus (IAF) tissue stained with H&E. (A) Non-degenerated spondylolisthesis (grade 2) disc. Scale bar: 50 μm. (B) Herniated disc. Scale bar: 100 μm. Note the rounded cell morphology and the prevalence of small cell clusters (arrows) which are larger in (B).

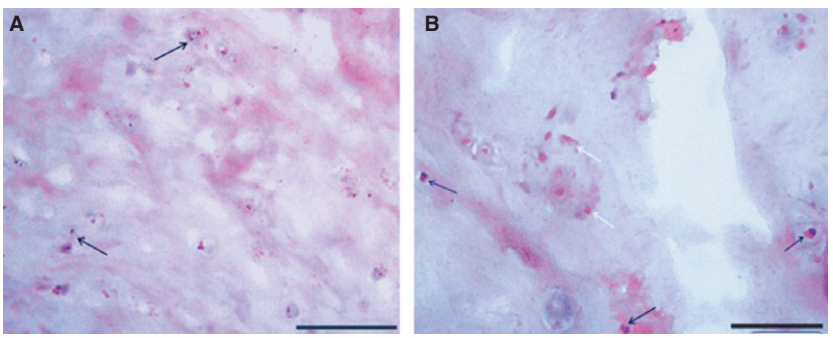

Fig. 3 Nucleus pulposus (NP) tissue stained with H&E. (A) Non-degenerated disc. Scale bar: 30 m. (B) Degenerated disc with cell clusters around a matrix fissure. Scale bar: 100 m. Note the amorphous matrix in both images, and the larger cell clusters in (B). White arrows indicate cells with disrupted cell membranes and some loss in nuclear stain, in contrast to cells with distinct nuclear and cytoplasmic staining (black arrows).

inflammatory cells, blood vessels and fibroblast-like cells. IAF regions of herniated and degenerated discs showed abundant cell clusters, especially near fissures (Fig. 2B). Clusters were also abundant within NP regions of these discs, and a few cells showed characteristic features of nuclear shrinkage with disrupted or lysed cell membranes (Fig. 3B).

Histological characterization of blood vessels

In all patient groups, blood vessels were localized chiefly around the disc periphery or where tissue was fibrous and delaminated, and showing evident loss of GAG, often accompanied by inflammatory cell invasion (Fig. 4). Blood vessels were formed of a single layer of endothelial cells without any muscle fibres. No blood vessels were observed within NP tissue. The occurrence of blood vessels varied between the four patient groups: blood vessels were identified within IAF or OAF tissue in 80% of HD/S discs, 46% of HD/NS discs and 27% of the D&S discs. In scoliotic discs (SD), vessels were observed only within the ligamentous regions surrounding the OAF. Blood vessels were always near or within fissures, but not all fissured or delaminated regions contained blood vessels. When all 40 discs were pooled, Spearman rank correlation between scores for blood vessels and tears was significant in IAF ($r_s = 0.75$, $P < 0.001$) and OAF ($r_s = 0.69$, $P < 0.0003$) tissues.

Toluidine blue staining and degenerative changes

Toluidine blue staining showed that GAG loss varied significantly between different patient groups and tissue types. Toluidine blue staining was depleted in severely disrupted IAF and OAF in comparison with NP. The highest scores for histopathological abnormalities (Table 2) were in HD/S patients and concerned the following: loss of GAGs ($P < 0.003$), development of tears containing inflammatory cells ($P < 0.004$) and increased blood vessel numbers ($P < 0.003$). Such changes usually occurred together in disrupted IAF and OAF regions (Fig. 4). HD/NS and D&S discs showed moderate GAG loss, whereas scoliotic disc samples showed the least GAG loss and fissuring. Loss of GAG was correlated with increased fissuring in the NP ($r_s = 0.88$, $P < 0.001$), IAF ($r_s = 0.74$, $P < 0.001$) and OAF ($r_s = 0.85$, $P < 0.001$).

Quantification of blood vessels and nerves using immunofluorescence

The density of blood vessels and nerves was greatest in OAF and IAF regions of discs from HD/S patients. Often, they appeared to track physical features in the matrix (Fig. 5). Analysis of serial Z-stacks of 30-μm-thick sections with VOLOCITY software showed small nerves as dots in a transverse 2-D plane, but with 3-D analysis such nerves were observed to be punctuate, arborising and not always straight in their course (Fig. 6). Of HD/NS specimens, 50% showed CD-31, PGP 9.5 or Substance P immunoreactivity in the IAF or OAF regions, and those specimens that did not. were confirmed by histology to consist predominantly of NP. Only 3/11 D&S specimens showed blood vessels and nerves within IAF or OAF regions. In all four patient groups, Substance-P immunoreactive nerves (Fig. 6) were adjacent to blood vessels or infiltrating inflammatory cells. Spondylolisthesis/degenerated (D&S) discs showed a few PGP 9.5 immunoreactive nerves in OAF regions, and control scoliosis (SD) discs showed them within ligaments, but no tissue from either of these two groups was immunopositive for Substance P. Quantitative data are summarised in Table 3. Statistical differences between tissues and patient groups are compiled in Table 4. Two-way ANOVA showed significant differences between patient groups for blood vessels ($P < 0.001$), nerve counts ($P = 0.004$) and the area occupied by blood vessels ($P = 0.002$), but comparisons between IAF and OAF regions showed insignificant differences for blood vessel counts ($P = 0.655$), nerve counts ($P = 0.345$) and distances from the nearest free surface of nerves immunoreactive for Substance P ($P = 0.105$) or PGP 9.5 ($P = 0.196$).

Correlation between GAG loss, blood vessels and nerves

When all tissue samples were pooled, Spearman rank correlation showed a significant relationship between GAG loss and (1) blood vessel count ($P = 0.03$, $r_s = 0.34$), (2) nerve count ($P = 0.02$, $r_s = 0.33$) and (3) area occupied by ingrowing blood vessels ($P = 0.02$, $r_s = 0.34$).

Maximum distances of blood vessels and nerves from free surfaces

In 30-μm-thick frozen sections, the maximum distance of nerves immunoreactive to Substance P and PGP 9.5 from the nearest free surface was 140 and 247 μm, respectively (Fig. 7). Blood vessels were always greater in number, grew deeper and occupied a larger areas compared with nerves (Fig. 8). The greatest area occupied by a single vessel was 57 910 μm^2 and the maximum distance of blood vessels from the nearest free surface was 888 μm. Nerves and blood vessels were greater in number and area in painful and structurally disrupted discs in comparison with non-disrupted scoliotic discs (Tables 3 and 4).

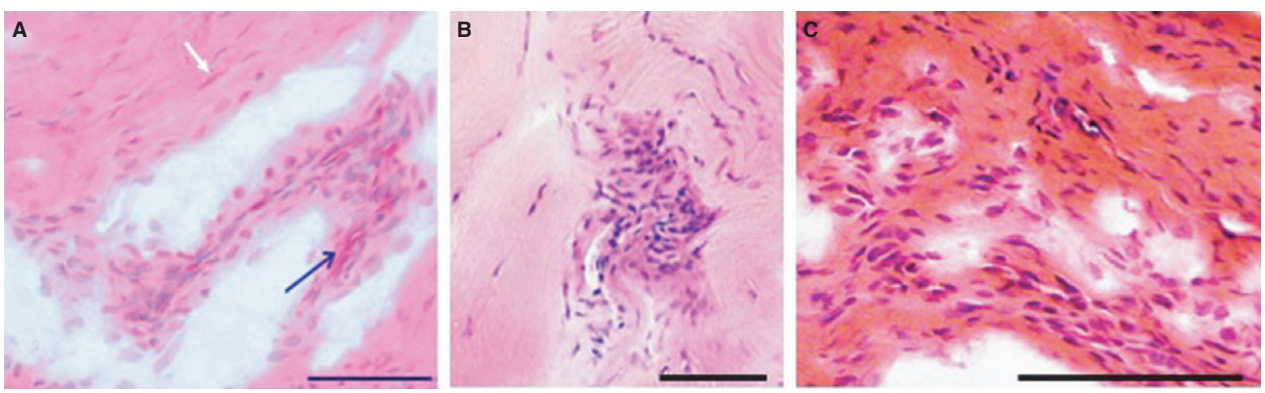

Fig. 4 Inflammatory cells in herniated annulus fibrosus. H&E stain. Scale bar: 50 μm. (A) Outer annulus fibrosus (OAF) tissue from a herniated disc with sciatica. Note the blood vessels in oblique transverse section (black arrow) together with inflammatory cells, and fibroblasts (white arrow). (B) Inner annulus fibrosus (IAF) tissue from a herniated disc without sciatica. Note the disorganised infolded lamellae. (C) Outer annulus fibrosus (OAF) tissue from a herniated disc with sciatica.

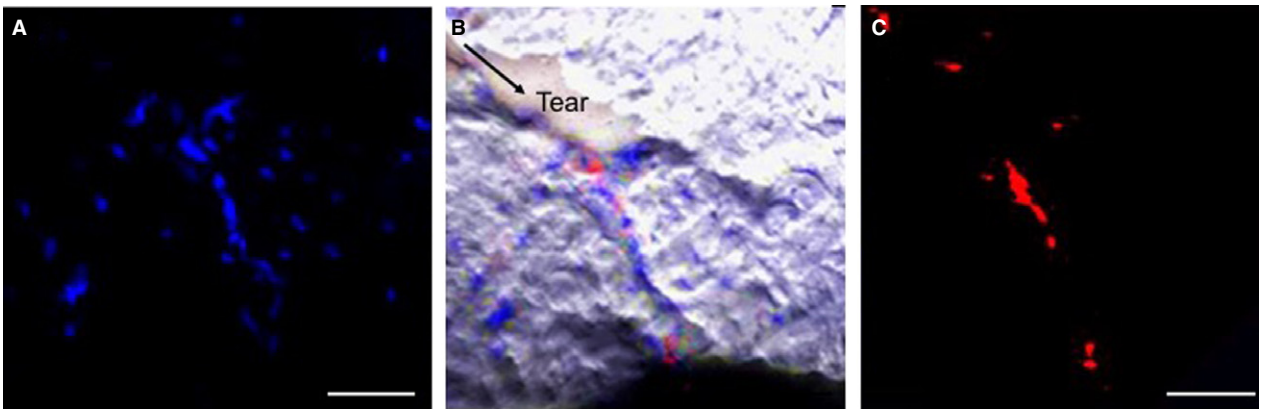

Fig. 5 Co-localisation of blood vessels and matrix defects in degenerated inner annulus fibrosus (IAF) tissue. Scale bar: 50 μm. (A) Cell nuclei stained blue with DAPI suggest blood vessels. (C) Blood vessel immunopositive to CD-31 shown in red. (B) Composite image showing blood vessels co-localised with a matrix tear as indicated by phase contrast imaging.

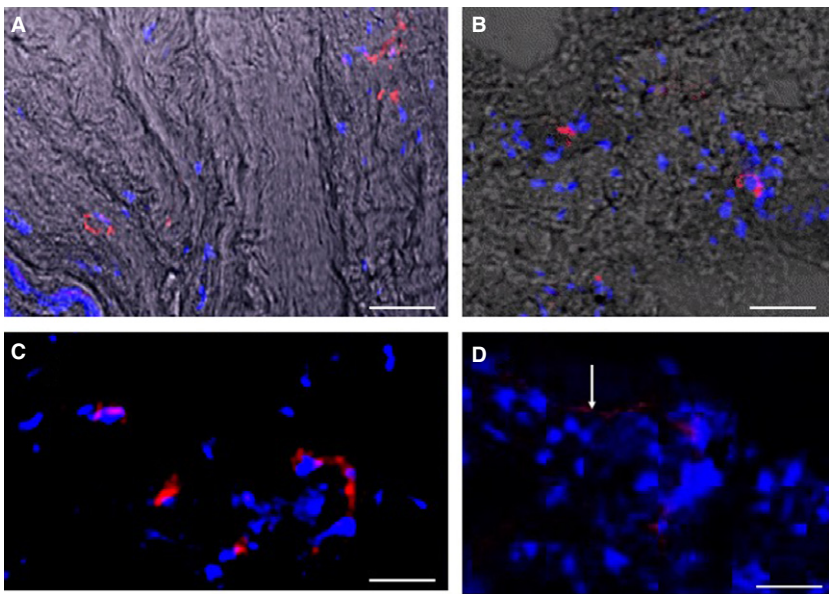

Fig. 6 Nerves in annulus tissues of herniated discs. Cell nuclei are stained blue with DAPI. Scale bar: 50 μm. (A) Fine nerves stained red for Substance P. Phase contrast imaging suggests matrix features. (B) Nerves stained red for PGP 9.5. (C) Nerves stained red for PGP 9.5. (D) Fine peripheral nerve (white arrow) stained red for Substance P.

Influence of Pfirrmann grade of disc degeneration

The area occupied by CD-31 immunopositive vessels correlated with Pfirrmann grade of disc degeneration ($r_s = 0.378$, $P < 0.02$) in the OAF region, and total nerve counts from both IAF and OAF regions correlated with the Pfirrmann grades ($r_s = 0.360$, $P < 0.02$).

Discussion

Summary of findings

Blood vessels and nerves were confined to physically disrupted and GAG-depleted annulus tissue, within 1 mm of a free surface. Their density increased with Pfirrman grade of disc degeneration, and with local GAG loss. Distinct (fragments of) blood vessels were greater in number, grew deeper, and occupied larger areas in comparison to nerves.

Study strengths and weaknesses

The use of surgically removed tissues from different patient groups, together with MRI images of the same discs, ensured clinical relevance. Combining immunofluorescence and confocal microscopy provided high resolution images which facilitated the identification of fine 3-D nerves and blood vessels within a dense matrix. Using multiple thick (30-μm) sections eliminated some artefacts of microtome sectioning (Claxton et al. 2010) and reduced the risk of missing something that really was present. ImageJ-analysis software yielded quantitative and objective results. Histological studies on the same tissue samples confirmed the presence of blood vessels and enabled immunostained structures to be located relative to features in the disc matrix. Finally, our clear images of nerves and blood vessels in the annulus (Figs 4–6) suggest that we did not experience difficulties with our antibodies (for Substance P, PGP 9.5 and CD-31).

Table 3 Quantitative data concerning nerves and blood vessels in 30-μm-thick sections.

	Patient groups											
	Scoliosis, *n* = 8			HD/S, *n* = 10			HD/NS, *n* = 11			D&S, *n* = 11		
Tissue type	N	IAF	OAF	NP	IAF	OAF	NP	IAF	OAF	NP	IAF	OAF
Blood vessels (count mm^{-2})	0	0	0	**0****	**4.5**** (3.2)	**8.2*** (6.5)	**0***	**1.9*** (1.8)	**2.5*** (0.7)	0	0.4 (0.9)	0.9 (1.9)
Blood vessel area (μm^2)	0	0	0	**0***	**19 558*** (13 517)	**25 677*** (24 043)	**0****	**2627**** (4628)	**7888**** (6710)	0	1597 (5221)	4788 (13 993)
Blood vessel distance (μm)	0	0	0	**0***	**197*** (131)	**305*** (276)	**0****	**66**** (88)	**290**** (248)	0	50 (113)	139 (252)
All nerves (count mm^{-2})	0	0	0	**0****	**2.1**** (1.6)	**2.6**** (2.0)	**0***	**0.6*** (1.0)	**1.5*** (0.7)	0	0.3 (0.7)	0.5 (1.1)
Sub P nerves distance (μm)	0	0	0	**0****	**45**** (29)	**37**** (33)	0	24 (50)	48 (16)	0	8.6 (25.9)	30.8 (55.8)
Sub P nerves max dist. (μm)	0	0	0	0	75	73	0	140	50		78	144
PGP 9.5 nerves distance (μm)	0	0	0	**0***	**71*** (87)	**62*** (82)	**0***	**48*** (73)	**121*** (12)	0	9.2 (23.5)	40 (78)
PGP 9.5 nerves max dist. (μm)	0	0	0	0	237	206	0	207	129	0	206	17.7

Sub P, substance P.
Data represent the mean
(SD), and are compared for three tissue types
(NP, IAF, OAF) and four patient groups.
Significant differences between the three tissue types are shown in bold, with significance levels denoted: $*P < 0.05$ or $**P < 0.01$. 'Distance' refers to distance from nearest free surface.

Table 4 Differences in quantitative data between the four patient groups, assessed separately for each tissue type.

Patient group	Blood vessels (count mm^{-2})	Blood vessels area (μm^2)	Blood vessel distance (μm)	All nerves (count mm^{-2})	Sub P nerves distance (μm)	PGP 9.5 nerves distance (μm)
HD/S						
HD/NS	**0.003**	**0.001**	**0.002**	0.256	0.630	0.953
D&S	**0.001**	**0.000**	**0.001**	0.123	0.760	0.835
SCOLI	**0.001**	**0.000**	**0.001**	**0.034**	**0.055**	**0.047**
HD/NS						
HD/S	**0.003**	**0.001**	**0.002**	0.256	0.630	0.953
D&S	0.986	0.979	0.556	0.978	0.996	0.506
SCOLI	0.816	0.892	0.912	0.675	0.536	**0.037**
D&S						
HD/S	**0.001**	**0.000**	**0.001**	0.123	0.760	0.835
HD/NS	0.986	0.979	0.556	0.978	0.996	0.506
SCOLI	0.942	0.985	0.922	0.872	0.413	0.195
SCOLI						
HD/S	**0.001**	**0.000**	**0.001**	**0.034**	**0.055**	**0.047**
HD/NS	0.816	0.892	0.912	0.675	0.536	**0.037**
D&S	0.942	0.985	0.991	0.872	0.413	0.195

Mean values are compared using univariate ANOVA with *post-hoc* Scheffe's test. Data are *P*-values, and significant differences ($P < 0.05$) between the four patient groups are shown in bold.

One weakness was the use of disc tissues from young idiopathic scoliosis patients to represent 'non-degenerated' controls. However, they provided a useful contrast with older and disrupted tissues from the other patient groups, and no other young tissues were available. Some matrix fissures may have been

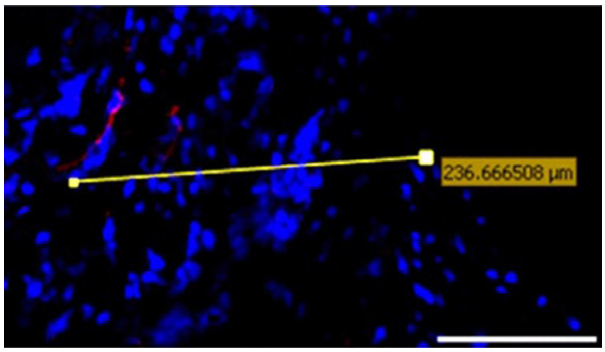

Fig. 7 VOLOCITY image analysis software was used to measure the furthest distance of each stained object (in this case a nerve immunostained for PGP 9.5) from the nearest free surface.

introduced during tissue removal and processing (Weiler et al. 2011), although co-localisation with GAG loss, cells and vascular structures suggests a natural origin. A limitation with the confocal system was that its high intensity irradiations reduced immunoreactivity after repeated or prolonged exposure. Finally, 'GAG-depletion' and 'physical disruption' (fissures and tears) were estimated only as categorical variables. However, we have shown previously that GAG content, quantified precisely using the DMMB assay, is 36–54% lower in disrupted annulus intact annulus from the same disc (Stefanakis et al. 2012).

Relationship to other studies

The present results are in broad agreement with most of the work summarised in the Introduction, and confirm that sensory nerves and blood vessels are common in degenerated and herniated discs removed at surgery. Our finding that blood vessels grow in further than nerves is supported by a previous study (Johnson et al. 2001). Results are compatible with the concept that cells in degenerated discs secrete growth factors such as VEGF and NGF (Purmessur et al. 2008; Binch et al. 2014) that encourage blood vessels and nerves to grow deeper (Burke et al. 2002; Johnson et al. 2006).

It is still not certain whether ingrowing blood vessels and nerves can reach the disc nucleus, even if the disc is severely degenerated and therefore decompressed (Adams et al. 1996b; Sato et al. 1999). Early work suggested they do not, and this is supported by later reports that blood vessels (on which nerves are presumed to depend) never grow in much beyond the outer-mid annulus (Johnson et al. 2001; Nerlich et al. 2007). On the other hand, Binch et al. support the previous work of Freemont et al. (1997) by showing that ingrowing nerves reach the nucleus in a substantial proportion of degenerated human discs and often are not associated with blood vessels (Binch et al. 2015). The present study identified nerves and blood vessels only in disrupted and proteoglycan-depleted *annulus* tissue, although this was sometimes located centrally in the disc. This apparent contradiction can be explained in terms of 'internal disc disruption' within severely degenerated discs (Crock 1986) whereby physical disruption can allow annulus lamellae to collapse into the decompressed nucleus cavity (Gunzburg et al. 1992; Adams et al. 2000), giving a false impression that nerves have grown into nucleus tissue. We sought to avoid this difficulty in the present study by classifying all results according to tissue type (NP, IAF, OAF). Technical difficulties may also account for some disagreement because it is difficult to identify thin filamentous structures within a dense and extensive collagenous matrix, and different antibodies have been used in various studies. However, this would not explain our inability to identify blood vessels within nucleus tissue in the present study, as these were plainly identifiable without antibodies (Fig. 4).

Explanation of results

Various cytokines and growth factors can promote the ingrowth of blood vessels and nerves (Ohtori et al. 2015), but it is simpler to consider what *prevents* such ingrowth. The two major blocks are physical (fluid) pressure and GAG concentration. High fluid pressure (above systolic blood pressure) would collapse hollow capillaries and prevent their ingrowth, although there is no evidence that pressure excludes nerves or other cells. GAGs inhibit the growth of nerve axons *in vitro* in a concentration-dependent manner

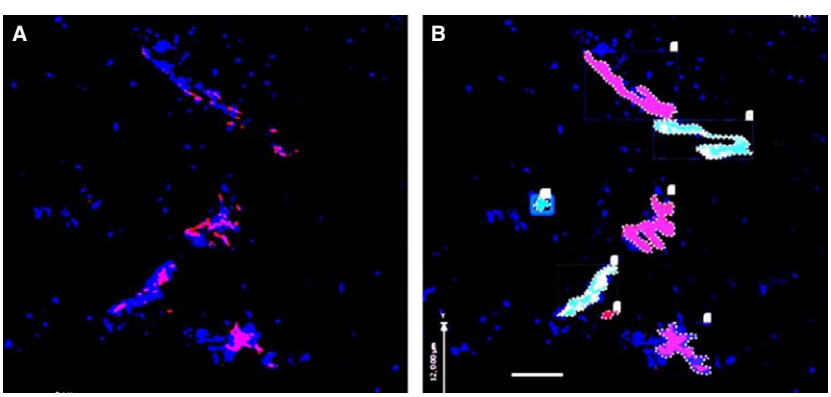

Fig. 8 Quantification of blood vessels in inner annulus fibrosus tissue (IAF) of a herniated disc using confocal microscopy. (A) Blood vessel(s) immunostained red for CD-31. Cell nuclei stained blue by DAPI. Scale bar: 100 µm. (B) VOLOCITY image analysis software was used to identify stained objects, count them, colour-code them, and measure the area occupied by each.

(Johnson et al. 2002; Purmessur et al. 2015), and similarly inhibit migration of endothelial cells (Johnson et al. 2005), which give rise to blood vessels. These physical and chemical influences are not entirely independent because GAGs attract water into disc tissue (Antoniou et al. 2004) and water content influences fluid pressure (Adams et al. 1996a).

In a young and non-degenerated human disc, GAG content is high in the nucleus but falls by approximately 70% in the outer annulus (Antoniou et al. 1996), and high fluid pressure is measurable in all regions except the outer 1–3 mm of annulus (Adams et al. 1996b). This may explain why healthy young discs contain no nerves, and why blood vessels are confined to the peripheral annulus. By age 60 years, typical GAG concentration falls by 50% in the nucleus and by 25% in the outer annulus (Antoniou et al. 1996). Fluid pressure typically falls by 10% in the nucleus and *increases* by a similar amount in the annulus, and the functional annulus expands slightly to encroach on the nucleus (Adams et al. 1996b). These changes evidently allow blood vessels and nerves to grow further into the annulus (Palmgren et al. 1999), but not into nucleus tissue (Nerlich et al. 2007). Much greater changes are seen when a disc becomes herniated or severely degenerated: then, nucleus pressure falls to very low levels (Adams et al. 1996b; Sato et al. 1999), high stress concentrations can arise in the annulus (Adams et al. 1996b) and GAG concentrations in the nucleus fall by a further 50% (Antoniou et al. 1996). In such discs, nerves and blood vessels can be found even in the nucleus (Binch et al. 2015).

The spatial pattern of re-vacularisation and re-innervation of a degenerated disc depends on the nature of structural disruption within it. We suggest three main patterns. First, in 'annulus-driven' disc degeneration (Adams & Dolan, 2012), the presence of one or more radial fissures in the annulus would allow blood vessels and nerves to track down a fissure from the periphery, possibly as far as the nucleus (Peng et al. 2006), which is where radial fissures originate from (Adams & Hutton, 1985). Annulus fissures are physically and chemically conducive to such ingrowth because their opposing 'free' surfaces allow a substantial loss of GAG, and physical pressure, for a distance of several hundred microns from the fissure axis (Stefanakis et al. 2012). Focal GAG loss leaves collagen-rich surfaces which can encourage cell migration (Johnson et al. 2005), and the associated focal loss of fluid pressure may permit blood vessel ingrowth also. This could explain why, in the present study, in-growing blood vessels and nerves were always in disrupted and proteoglycan-depleted annulus, < 1 mm from the nearest free surface. Previous authors also have reported blood vessels and nerves invading radial fissures in human (Peng et al. 2006; Vernon-Roberts et al. 2007; Shan et al. 2017) and animal (Xin et al. 2017) discs. The second re-vacularisation and re-innervation pattern affects 'endplate-driven' disc degeneration when there is damage to one or both vertebral endplates (Adams & Dolan, 2012) which greatly decompresses the disc nucleus (Dolan et al. 2013). An intact cartilage endplate, in particular, does not appear to permit blood vessels or nerves to grow through it (Nerlich et al. 2007; Lama et al. 2014), but the presence of a structural defect could conceivably allow vertical growth into the decompressed nucleus (Freemont et al. 2002). Any such nerves may have been overlooked in the present study if they were short, or if the cartilage endplate was not included in the surgically retrieved disc sample. A third pattern of re-vacularisation and re-innervation is evident if a degenerated disc herniates (prolapses). Then, displaced fragments of nucleus and/or annulus escape the pressurised confines of the disc and swell rapidly, allowing their GAGs to escape (Dolan et al. 1987). The resulting collagenous tissue can then be covered, and subsequently invaded from all sides, by blood vessels and nerves, so that the herniation is eventually 'resorbed' (Gronblad et al. 2000). Similar events probably explain most of the differences between 'HD' and 'D&S' discs in the present study.

The above discussion indicates that distributions of blood vessels and nerves within degenerated intervertebral discs depend very much on the nature of structural disruption in the disc and endplates, as well as on age and GAG content.

Clinical relevance

Nociceptive nerves within human discs could cause chronic discogenic pain if they become 'sensitised', most likely by inflammatory changes or bacterial infection. Neuropeptides such as Substance P, CGRP and VIP (Ashton et al. 1994b; Brown et al. 1997; Coppes et al. 1997; Edgar, 2007) play an important role in neurogenic inflammation and vasodilation of blood vessels (Goupille et al. 1998), and discogenic pain is closely associated with pro-inflammatory cytokines such as the interleukins (Risbud & Shapiro, 2014; Altun, 2016) and tumour necrosis factor alpha (TNFα; Lai et al. 2016). Probably, inflammatory cells enter disc tissues along the same defects as blood vessels (Fig. 4) and are stimulated to release mediators such as phospholipase A2, prostaglandin E2 and nitric oxide (Saal et al. 1990; Gronblad et al. 1994; Saal, 1995; Kang et al. 1996, 1997; Habtemariam et al. 1998). Inflammatory cells also synthesise, store and secrete nerve growth factors, which promote nerve ingrowths into more central regions of the discs (Peng et al. 2006). Disc nerves could also be sensitised by anaerobic bacteria, which are present in many degenerated and herniated discs (Albert et al. 2013a), where they appear to cause severe and chronic back pain (Albert et al. 2013b).

Unanswered questions

The present results suggest a spatial association between disc nerves and blood vessels, but they do not prove that

disc nerves require adjacent blood vessels, or demonstrate which grow in first.

Conclusion

The present study shows clearly where small nerves and blood vessels are present within disc tissues, and where they are absent. Results support our hypothesis and suggest that nerve and blood vessel ingrowth into degenerated human discs is largely confined to physically disrupted and proteoglycan-depleted regions of tissue.

Acknowledgements

This work was funded in the UK by Action Medical Research, and by a PhD studentship (for P.L.) from the State Government of Sikkim, India.

Author contributions

P.L.: Experimental design and methods; experimental work and interpretation of results; manuscript preparation. C.L.M.: Experimental design and methods; interpretation of results; manuscript preparation. I.J.H.: Surgical tissues; experimental design; advice concerning clinical relevance. P.D.: Experimental design; interpretation of results; manuscript preparation. M.A.A.: Experimental design; interpretation of results; manuscript preparation.

Ethics

Research approved by the NRES Ethics Committee, Frenchay Hospital, Bristol, UK.

References

Adams MA, Dolan P (2012) Intervertebral disc degeneration: evidence for two distinct phenotypes. *J Anat* **221**, 497–506.

Adams MA, Hutton WC (1985) Gradual disc prolapse. *Spine* **10**, 524–531.

Adams MA, McMillan DW, Green TP, et al. (1996a) Sustained loading generates stress concentrations in lumbar intervertebral discs. *Spine* **21**, 434–438.

Adams MA, McNally DS, Dolan P (1996b) 'Stress' distributions inside intervertebral discs. The effects of age and degeneration. *J Bone Joint Surg Br* **78**, 965–972.

Adams MA, Freeman BJ, Morrison HP, et al. (2000) Mechanical initiation of intervertebral disc degeneration. *Spine* **25**, 1625–1636.

Albert HB, Lambert P, Rollason J, et al. (2013a) Does nuclear tissue infected with bacteria following disc herniations lead to Modic changes in the adjacent vertebrae? *Eur Spine J* **22**, 690–696.

Albert HB, Sorensen JS, Christensen BS, et al. (2013b) Antibiotic treatment in patients with chronic low back pain and vertebral bone edema (Modic type 1 changes): a double-blind randomized clinical controlled trial of efficacy. *Eur Spine J* **22**, 697–707.

Altun I (2016) Cytokine profile in degenerated painful intervertebral disc: variability with respect to duration of symptoms and type of disease. *Spine J* **16**, 857–861.

Antoniou J, Steffen T, Nelson F, et al. (1996) The human lumbar intervertebral disc: evidence for changes in the biosynthesis and denaturation of the extracellular matrix with growth, maturation, ageing, and degeneration. *J Clin Invest* **98**, 996–1003.

Antoniou J, Demers CN, Beaudoin G, et al. (2004) Apparent diffusion coefficient of intervertebral discs related to matrix composition and integrity. *Magn Reson Imaging* **22**, 963–972.

Aoki Y, Ohtori S, Takahashi K, et al. (2004) Innervation of the lumbar intervertebral disc by nerve growth factor-dependent neurons related to inflammatory pain. *Spine* **29**, 1077–1081.

Ashton IK, Roberts S, Jaffray DC, et al. (1994a) Neuropeptides in the human intervertebral disc. *J Orthop Res* **12**, 186–192.

Ashton IK, Walsh DA, Polak JM, et al. (1994b) Substance P in intervertebral discs: binding sites on vascular endothelium of the human annulus fibrosus. *Acta Orthop* **65**, 635–639.

Baschong W, Suetterlin R, Laeng RH (2001) Control of autofluorescence of archival formaldehyde-fixed, paraffin-embedded tissue in confocal laser scanning microscopy (CLSM). *J Histochem Cytochem* **49**, 1565–1571.

Binch AL, Cole AA, Breakwell LM, et al. (2014) Expression and regulation of neurotrophic and angiogenic factors during human intervertebral disc degeneration. *Arthritis Res Ther* **16**, 416.

Binch AL, Cole AA, Breakwell LM, et al. (2015) Nerves are more abundant than blood vessels in the degenerate human intervertebral disc. *Arthritis Res Ther* **17**, 370.

Boden SD, Davis DO, Dina TS, et al. (1990) Abnormal magnetic-resonance scans of the lumbar spine in asymptomatic subjects. A prospective investigation. *J Bone Joint Surg Am* **72**, 403–408.

Bogduk N, Tynan W, Wilson AS (1981) The nerve supply to the human lumbar intervertebral discs. *J Anat* **132**, 39–56.

Boos N, Rieder R, Schade V, et al. (1995) The diagnostic accuracy of magnetic resonance imaging, work perception, and psychosocial factors in identifying symptomatic disc herniations: 1995 Volvo Award in clinical sciences.. *Spine* **20**, 2613–2625.

Boos N, Weissbach S, Rohrbach H, et al. (2002) Classification of age-related changes in lumbar intervertebral discs: 2002 Volvo Award in basic science. *Spine* **27**, 2631–2644.

Brown MF, Hukkanen MV, McCarthy ID, et al. (1997) Sensory and sympathetic innervation of the vertebral endplate in patients with degenerative disc disease. *J Bone Joint Surg Br* **79**, 147–153.

Bruehlmann SB, Rattner JB, Matyas JR, et al. (2002) Regional variations in the cellular matrix of the annulus fibrosus of the intervertebral disc. *J Anat* **201**, 159–171.

Burke JG, Watson RWG, McCormack D, et al. (2002) Spontaneous production of monocyte chemoattractant protein-1 and interleukin-8 by the human lumbar intervertebral disc. *Spine* **27**, 1402–1407.

Cheung KM, Karppinen J, Chan D, et al. (2009) Prevalence and pattern of lumbar magnetic resonance imaging changes in a population study of one thousand forty-three individuals. *Spine* **34**, 934–940.

Claxton N, Fellers T, Davidson M (2010). Laser scanning confocal microscopy. Department of Optical Microscopy and Digital Imaging, National High Magnetic Field Laboratory, Florida State University, 37 p., Unpublished (http://www.olympusfluoview.com/theory/LSCMIntro.pdf) & https://doi.org/10.1002/0471732877.

Coppes MH, Marani E, Thomeer RT, et al. (1997) Innervation of 'painful' lumbar discs. *Spine* **22**, 2342–2349; discussion 2349-50.

Crock HV AO (1986). The Presidential Address: ISSLS: Internal Disc Disruption A Challenge to Disc Prolapse Fifty Years On. *Spine* **11** (6), 650–653.

Dolan P, Adams MA, Hutton WC (1987) The short-term effects of chymopapain on intervertebral discs. *J Bone Joint Surg Br* **69**, 422–428.

Dolan P, Luo J, Pollintine P, et al. (2013) Intervertebral disc decompression following endplate damage: implications for disc degeneration depend on spinal level and age. *Spine (Phila Pa 1976)* **38**, 1473–1481.

Edgar MA (2007) The nerve supply of the lumbar intervertebral disc. *J Bone Joint Surg Br* **89-B**, 1135–1139.

Fields AJ, Liebenberg EC, Lotz JC (2014) Innervation of pathologies in the lumbar vertebral end plate and intervertebral disc. *Spine J* **14**, 513–521.

Freemont AJ, Peacock TE, Goupille P, et al. (1997) Nerve ingrowth into diseased intervertebral disc in chronic back pain. *Lancet* **350**, 178–181.

Freemont AJ, Watkins A, le Maitre C, et al. (2002) Nerve growth factor expression and innervation of the painful intervertebral disc. *J Pathol* **197**, 286–292.

Goupille P, Jayson MIV, Valat J-P, et al. (1998) The role of inflammation in disk herniation-associated radiculopathy. *Semin Arthritis Rheum* **28**, 60–71.

Gronblad M, Virri J, Tolonen J, et al. (1994) A controlled immunohistochemical study of inflammatory cells in disc herniation tissue. *Spine (Phila Pa 1976)* **19**, 2744–2751.

Gronblad M, Virri J, Seitsalo S, et al. (2000) Inflammatory cells, motor weakness, and straight leg raising in transligamentous disc herniations. *Spine* **25**, 2803–2807.

Gunzburg R, Parkinson R, Moore R, et al. (1992) A cadaveric study comparing discography, magnetic resonance imaging, histology, and mechanical behavior of the human lumbar disc. *Spine* **17**, 417–426.

Habtemariam A, Gronblad M, Virri J, et al. (1998) A comparative immunohistochemical study of inflammatory cells in acute-stage and chronic-stage disc herniations. *Spine* **23**, 2159–2165; discussion 2166.

Johnson WE, Evans H, Menage J, et al. (2001) Immunohistochemical detection of Schwann cells in innervated and vascularized human intervertebral discs. *Spine (Phila Pa 1976)* **26**, 2550–2557.

Johnson WE, Caterson B, Eisenstein SM, et al. (2002) Human intervertebral disc aggrecan inhibits nerve growth in vitro. *Arthritis Rheum* **46**, 2658–2664.

Johnson WE, Caterson B, Eisenstein SM, et al. (2005) Human intervertebral disc aggrecan inhibits endothelial cell adhesion and cell migration in vitro. *Spine* **30**, 1139–1147.

Johnson WEBP, Sivan SP, Wright KTB, et al. (2006) Human intervertebral disc cells promote nerve growth over substrata of human intervertebral disc aggrecan. *Spine* **31**, 1187–1193.

Kang JD, Georgescu HI, McIntyre-Larkin L, et al. (1996) Herniated lumbar intervertebral discs spontaneously produce matrix metalloproteinases, nitric oxide, interleukin-6, and prostaglandin E2. *Spine* **21**, 271–277.

Kang JD, Stefanovic-Racic M, McIntyre LA, et al. (1997) Toward a biochemical understanding of human intervertebral disc degeneration and herniation. Contributions of nitric oxide, interleukins, prostaglandin E2, and matrix metalloproteinases. *Spine* **22**, 1065–1073.

Lai A, Moon A, Purmessur D, et al. (2016) Annular puncture with tumor necrosis factor-alpha injection enhances painful behavior with disc degeneration in vivo. *Spine J* **16**, 420–431.

Lama P, Le Maitre CL, Dolan P, et al. (2013) Do intervertebral discs degenerate before they herniate, or after? *Bone Joint J* **95-B**, 1127–1133.

Lama P, Zehra U, Balkovec C, et al. (2014) Significance of cartilage endplate within herniated disc tissue. *Eur Spine J* **23**, 1869–1877.

Maatta JH, Karppinen J, Paananen M, et al. (2016) Refined phenotyping of modic changes: imaging biomarkers of prolonged severe low back pain and disability. *Medicine (Baltimore)* **95**, e3495.

Nerlich AG, Schaaf R, Walchli B, et al. (2007) Temporo-spatial distribution of blood vessels in human lumbar intervertebral discs. *Eur Spine J* **16**, 547–555.

Ohtori S, Inoue G, Miyagi M, et al. (2015) Pathomechanisms of discogenic low back pain in humans and animal models. *Spine J* **15**, 1347–1355.

Palmgren T, Gronblad M, Virri J, et al. (1999) An immunohistochemical study of nerve structures in the anulus fibrosus of human normal lumbar intervertebral discs. *Spine* **24**, 2075–2079.

Peng B, Wu W, Hou S, et al. (2005) The pathogenesis of discogenic low back pain. *J Bone Joint Surg Br* **87**, 62–67.

Peng B, Hao J, Hou S, et al. (2006) Possible pathogenesis of painful intervertebral disc degeneration. *Spine* **31**, 560–566.

Pfirrmann CW, Metzdorf A, Zanetti M, et al. (2001) Magnetic resonance classification of lumbar intervertebral disc degeneration. *Spine* **26**, 1873–1878.

Purmessur D, Freemont AJ, Hoyland JA (2008) Expression and regulation of neurotrophins in the nondegenerate and degenerate human intervertebral disc. *Arthritis Res Ther* **10**, R99.

Purmessur D, Cornejo MC, Cho SK, et al. (2015) Intact glycosaminoglycans from intervertebral disc-derived notochordal cell-conditioned media inhibit neurite growth while maintaining neuronal cell viability. *Spine J* **15**, 1060–1069.

Risbud MV, Shapiro IM (2014) Role of cytokines in intervertebral disc degeneration: pain and disc content. *Nat Rev Rheumatol* **10**, 44–56.

Roberts S, Eisenstein SM, Menage J, et al. (1995) Mechanoreceptors in intervertebral discs. Morphology, distribution, and neuropeptides [see comments]. *Spine* **20**, 2645–2651.

Saal JS (1995) The role of inflammation in lumbar pain. *Spine* **20**, 1821–1827.

Saal JS, Franson RC, Dobrow R, et al. (1990) High levels of inflammatory phospholipase A2 activity in lumbar disc herniations. *Spine (Phila Pa 1976)* **15**, 674–678.

Sato K, Kikuchi S, Yonezawa T (1999) In vivo intradiscal pressure measurement in healthy individuals and in patients with ongoing back problems. *Spine* **24**, 2468–2474.

de Schepper EI, Damen J, van Meurs JB, et al. (2010) The association between lumbar disc degeneration and low back pain: the influence of age, gender, and individual radiographic features. *Spine (Phila Pa 1976)* **35**, 531–536.

Shan Z, Chen H, Liu J, et al. (2017) Does the high-intensity zone (HIZ) of lumbar intervertebral discs always represent an annular fissure? *Eur Radiol* **27**, 1267–1276.

Stefanakis M, Al-Abbasi M, Harding I, et al. (2012) Annulus fissures are mechanically and chemically conducive to the ingrowth of nerves and blood vessels. *Spine (Phila Pa 1976)* **37**, 1883–1891.

Tolofari SK, Richardson SM, Freemont AJ, et al. (2010) Expression of semaphorin 3A and its receptors in the human intervertebral disc: potential role in regulating neural ingrowth in the degenerate intervertebral disc. *Arthritis Res Ther* **12**, R1.

Vernon-Roberts B, Moore RJ, Fraser RD (2007) The natural history of age-related disc degeneration: the pathology and sequelae of tears. *Spine (Phila Pa 1976)* **32**, 2797–2804.

Videman T, Nurminen M (2004) The occurrence of anular tears and their relation to lifetime back pain history: a cadaveric study using barium sulfate discography. *Spine* **29**, 2668–2676.

Vo NV, Hartman RA, Patil PR, et al. (2016) Molecular mechanisms of biological aging in intervertebral discs. *J Orthop Res* **34**, 1289–1306.

Wang Y, Videman T, Battie MC (2012) ISSLS prize winner: lumbar vertebral endplate lesions: associations with disc degeneration and back pain history. *Spine (Phila Pa 1976)* **37**, 1490–1496.

Weiler C, Lopez-Ramos M, Mayer H, et al. (2011) Histological analysis of surgical lumbar intervertebral disc tissue provides evidence for an association between disc degeneration and increased body mass index. *BMC Res Notes* **4**, 497.

Xin L, Xu W, Yu L, et al. (2017) Effects of annulus defects and implantation of poly(lactic-co-glycolic acid) (PLGA)/fibrin gel scaffolds on nerves ingrowth in a rabbit model of annular injury disc degeneration. *J Orthop Surg Res* **12**, 73.